



A simple, universal and multifunctional template agent for personalized treatment of bone tumors

Wei-bo Liu^{a,1}, Su-he Dong^{c,1}, Wen-hao Hu^a, Meng Gao^d, Teng Li^a, Quan-bo Ji^a,
Xiao-qing Yang^a, Deng-bin Qi^a, Zhen Zhang^a, Ze-Long Song^a, Yu-jie Liu^{b,1,**},
Xue-song Zhang^{a,*}

^a Department of Orthopaedics, The Fourth Medical Centre, Chinese PLA General Hospital, 51 Fucheng Road, Haidian District, Beijing, 100048, China

^b Department of Orthopedic Oncology and Spine Tumor Center, Changzheng Hospital, Second Military Medical University, Shanghai, 200001, China

^c PLA Rocket Force Characteristic Medical Center, Beijing, 100088, China

^d School of Medicine, Nankai University, Tianjin, 300071, China

ARTICLE INFO

Keywords:

Bone tumor
Osteosarcoma
Polydopamine
Photothermal therapy

ABSTRACT

Bone tumors occur in bone or its accessory tissues. Benign bone tumors are easy to cure and have good prognosis, while malignant bone tumors develop rapidly and have poor and high mortality. So far, there is no satisfactory treatment method. Here, we designed a universal template vector for bone tumor therapy that simultaneously meets the needs of bone targeting, tumor killing, osteoclast suppression, and tumor imaging. The template is composed of a polydopamine (PDA) core and a multifunctional surface. PDA has excellent biosafety and photothermal performance. In this study, alendronate sodium (ALN) is grafted to enable its general bone targeting function. PDA core can carry a variety of chemotherapy drugs, and the rich ALN group can carry a variety of metal ions with an imaging function. Therefore, more personalized treatment plans can be designed for different bone tumor patients. In addition, the PDA core enables photothermal therapy and enhanced chemotherapy. Through template drug Doxorubicin (DOX) and template imaging ion Fe (II), we systematically verified the therapeutic effect, imaging effect, and inhibition of bone dissolution of the agent on Osteosarcoma (OS), a primary malignant bone tumor, *in vivo*. In conclusion, our work provides a more general template carrier for the clinical treatment of bone tumors, through which personalized treatment of bone tumors can be achieved.

1. Introduction

Malignant tumors have become one of the most lethal diseases in clinical these years [1]. In particularly, Osteosarcoma (OS), the most common malignant bone tumor accounting for about 35% of malignant bone tumors along with local invasiveness and distant metastases [2], has been still a challenge and seriously threatened the health of children, adolescents and young adults [3,4]. OS often occurs in the long bones with abundant blood flow marked as primary tumor (starting in long bones or cartilages) or metastatic tumor (starting elsewhere of body and spreading to the bone), which manifests as poor prognosis, high recurrence rates and low survival rates [5]. Furthermore, there are no apparent clinical features in the early stage of OS, so that it is difficult to

diagnose and treat quickly [6]. In recent decades, the technology of treatment has developed dramatically and the prognosis of OS has improved significantly [7]. However, only 40%–60% is the five-year survival rate raised to Ref. [8]. Nowadays, effective clinical treatments for OS include surgery, radiation therapy and chemotherapy, although each has its limitations. Chemotherapy has often been taken up first in the majority of OS patients, even though it easily causes drug resistance and even confront the recurrence and metastasis [9]. Surgical treatment is mainly used following chemotherapy of OS resection, which is challenging to clear away tumor cells completely and often leads to bone defects [10], and after which there always has been a long term chemotherapy period. In addition, OS cells are not sensitive to radiotherapy, and large doses of radiation could cause damages to normal

Peer review under responsibility of KeAi Communications Co., Ltd.

* Corresponding author.

** Corresponding author.

E-mail addresses: yujieliu16@163.com (Y.-j. Liu), zhangxuesong301@126.com (X.-s. Zhang).

¹ These authors as co-first author contributed equally to this work.

<https://doi.org/10.1016/j.bioactmat.2021.10.027>

Received 30 August 2021; Received in revised form 13 October 2021; Accepted 18 October 2021

Available online 26 October 2021

2452-199X/© 2022 The Authors. Publishing services by Elsevier B.V. on behalf of KeAi Communications Co. Ltd. This is an open access article under the CC

BY-NC-ND license (<http://creativecommons.org/licenses/by-nc-nd/4.0/>).

tissues [11]. Thus, it is urgent to develop novel strategies to hedge the defects and limitations of existing methods and improve the curative effect of OS in clinical.

Photothermal therapy (PTT) is a novel strategy for OS treatment [12, 13], which performs photothermal agents to convert near-infrared (NIR) light into heat to exert cytotoxic on tumor cells [14], such as cell membrane damage [15], protein degeneration [16] and cell death or necrosis [17]. There are a lot of studies based on PTT for tumor therapy [15,18]. As a mild, selective, effective and non-invasive approach, PTT can be used to chemotherapy-resistant OS with excellent outcomes, which has inspired increasing attention from researchers [19]. Though PTT is debatable for clinical application on bone tumor, it is getting more and more attention because of its efficient function in killing tumor cells. More effective and safe improvements in PTT treatment will be the goal in future. The therapeutic effect of PTT is closely involved with photothermal agents and the light regions [20]. The NIR light region (700–1100 nm) fits PTT laser irradiation treatment because of its low scatter and absorption in soft tissues [21], and there have been some studies certifying the significant function of NIR on bone tumor [18], which indicated the NIR can penetrate the skin and bone tissue to kill the tumor cells. Photothermal agents for tumors are mainly based on carbon and metal element, including carbon nanotubes [22], graphene [23], gold nanostructures [24], copper-based nanoplateforms [25], and organic-dye-based agents [26], among which bisphosphonate, oligopeptide, and aptamer can perform as bone-targeted agents to deliver them to lesions of bone. Although NIR-based photothermal agents have made some successful progress in OS treatment [27], certain inherent defects restrict their further clinical transformation and application, including low quantum yield [28], poor stability [29], low thermal stability [30], rapid blood clearance [31], and potential acute or chronic bio-toxicity [32]. Thus, various modification strategies have been proposed to improve intrinsic properties [29] (surface modification, element doping, and coating with osteogenic components) or to add functionality [23] (drug loading, cell-targeted vectors, biosensor techniques, and photothermal tumor ablation) of photothermal agents for OS treatments.

Polydopamine (PDA), as a kind of endogenous product, is the main component of the melanin, which has good biocompatibility, biodegradability, and low toxicity [33], and is widely distributed in various tissues and organs [34]. PDA contains various functional groups, including catechol, amine, and imine, easily modified with various substances [34]. PDA has been a candidate for photothermal agent owing to high photothermal conversion efficiency [35], which can damage tumor cells but normal cells in a short time NIR irradiation [36].

Alendronate (ALN), as a kind of typical bone-targeted bisphosphonates [37], can get copolymerization with *N*-(2-hydroxypropyl)-methacrylamide (HPMA) [38], which can accumulate in the bone tissue specifically [39]. PDA was used for assisting the ALN-based nanoparticle modification for application in PTT.

At present, among the frontline drugs of OS treatment, doxorubicin stands out due to its high therapeutic index [10]. However, conventional doxorubicin often has an uncontrolled release pattern and off-target effects, which limited its clinical application⁵¹. Recent efforts on nanoparticles have markedly improved the safety, tolerability, and therapeutic index, leading to doxorubicin accumulation within the tumor site [40]. When agents combine chemotherapy with PTT, a novel therapy has been created defined chemo-photothermal therapy (CPT), which has proven to be an optimal choice to improve the therapeutic efficacy of various tumors [41].

Herein, we instituted a bone-targeted multifunctional all-in-one nanoparticle, PDA-ALN/DOX, which was designed for the chemo-photothermal treatment of OS. The nanoparticle consisted of melanin-like polydopamine (PDA), alendronate (ALN), and doxorubicin (DOX), which presented high bone targeting properties, photothermal conversion efficiency, drug loading capacity, and multimodal imaging modalities. PDA-ALN/DOX can more effectively improve temperature

around the OS than simple PTT or chemotherapy. *In vivo*, tumor growth in PDA-ALN/DOX + NIR mice group was significantly suppressed. In addition, the Fe-loaded PDA-ALN (PDA-ALN/Fe) performed higher T1-weighted MRI in OS regions, which indicated the accumulation of the nanoparticles over tumor tissues. Therefore, this work provides a CPT agent PDA-ALN/DOX, as a remarkable therapeutic nanoparticle with significant clinical values.

2. Methods

2.1. Materials

Dopamine and doxorubicin were both bought from Sigma-Aldrich (USA). Alendronate, ferrous chloride, Tris, and Dimethylsulfoxide were purchased from Macklin Biochemical (Shanghai, China).

2.2. Prepare for PDA-ALN

PDA was acquired based on the method of literature reported. Generally, 8 mL ethanol was added into 18 mL H₂O bathing with magnetic stirring at 30 °C, then aqueous ammonia solution (0.6 mL) was appended into the aforementioned liquid lasting for 12 h. The reaction solution was centrifugated for 15 min at 15000 rpm and washed three times with H₂O to prepare PDA. Equal PDA and ALN were appended to alkaline buffer solution for 24 h with mildly magnetic stirring. The reaction solution was centrifugated for 15 min at 15000 rpm and washed three times with H₂O to prepare PDA-ALN.

2.3. Prepare for PDA/Fe and PDA-ALN/Fe

After the synthesis of PDA-ALN, ferrous chloride was added with magnetic stirring for 1 h at the mass ratio of 10:1, RT. Then the Fe-loaded PDA was centrifugated for 15 min at 15000 rpm, washed three times with H₂O, and detected by ICP-MS (Thermo, USA).

2.4. Prepare for PDA-ALN/DOX

DOX was coupled to PDA-ALN by adding 1.6 mg PDA-ALN and 0.32 mg DOX into an aqueous solution with magnetic stirring for 12 h RT. Then the reaction solution was centrifuged for 5 min at 2000 rpm, and collect the supernatant, continuously centrifuged for 10 min at 15000 rpm to prepare PDA-ALN/DOX. The UV absorption (Cary60, Agilent Technologies, USA) of PDA-ALN/DOX was detected to determine the drug loading capacity of PDA-ALN.

2.5. Characterization

TEM (HT7700, Hitachi, Japan, 100 KV), SEM (S4800, Hitachi, Japan, 10 kV), and HAADF-STEM were performed to take the images of nanoparticles. Zetasizer Nano ZS90 (Malvern, UK) was used to determine the hydrodynamic diameters and zeta potentials of nanoparticles.

2.6. Photothermal effect

Different concentration gradients of PDA or PDA-ALN were added in a 1 cm² cuvette and irradiated with an 808 nm NIR laser at 3.6 W/cm² for 10 min. The thermal infrared camera (Magnity Electronics, China) was used to monitor the temperature changes of PDA or PDA-ALN.

2.7. Stimuli-responsive drug release

PDA-ALN/DOX was added in a 1 cm² cuvette and irradiated with an 808 nm NIR laser at 3.6 W/cm² for several minutes (0, 5, 10, 20, 30 min). Then, the reaction solution was centrifuged for 10 min at 15000 rpm and collect the supernatant to analyze by UV absorption to determine the amount of DOX in the solution.

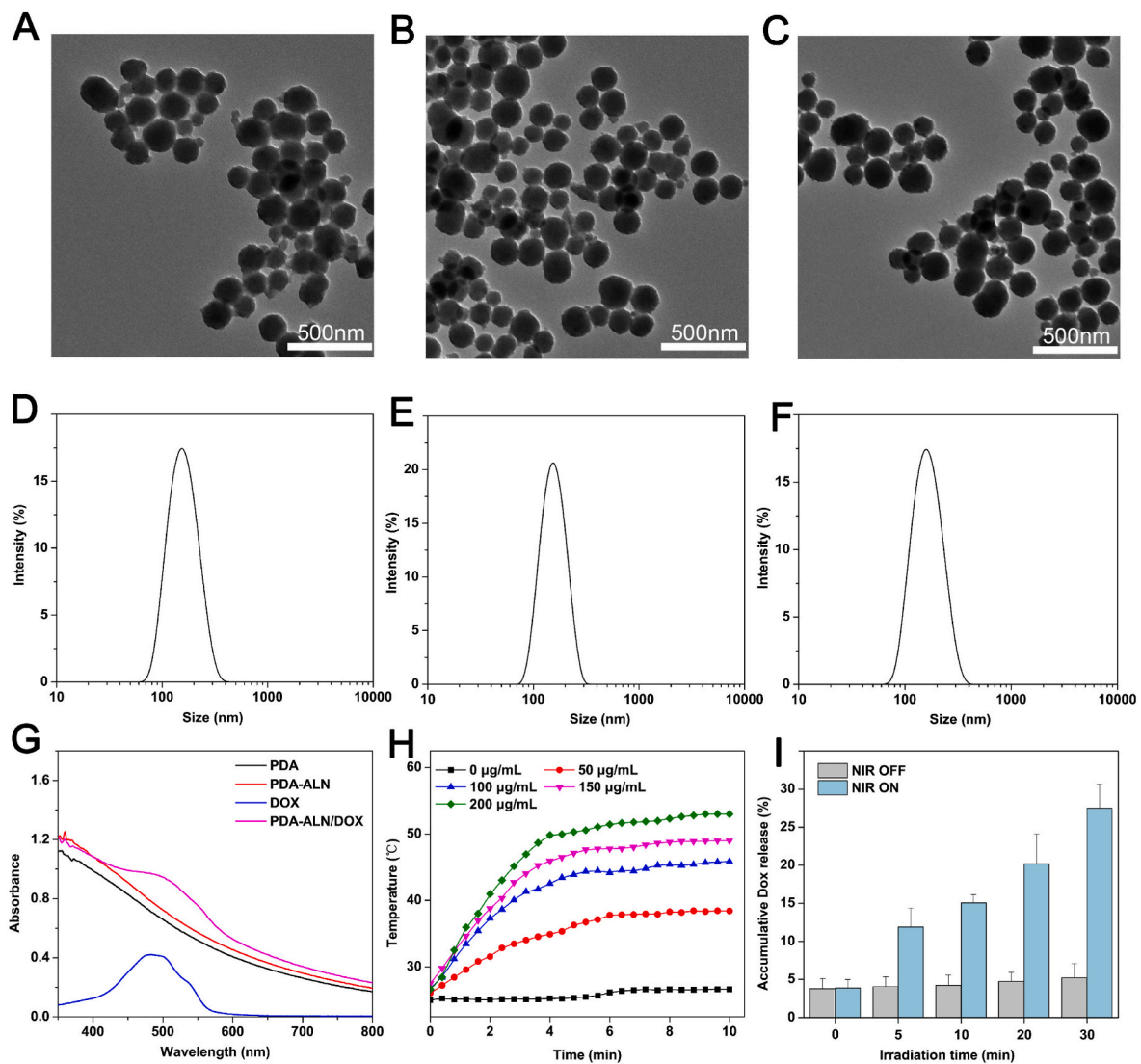


Fig. 1. Characterizations of PDA-ALN and PDA-ALN/DOX nanoparticles.

(A,D) TEM images and size distribution of PDA, PDA-ALN (B,E) and PDA-ALN/DOX (C,F). (G) UV-Vis spectra of PDA-ALN loaded with DOX. (H) Photothermal heating curves of PDA-ALN with different concentrations irradiated by NIR light at a power density of 3.6 W cm^{-2} . (I) The accumulative drug release from PDA-ALN/DOX with or without NIR irradiation at a power density of 3.6 W cm^{-2} for different times.

2.8. Cell culture

NIH3T3 cells (ATCC), 143B cells (ATCC) and U2OS cells (ATCC) were cultured in DMEM medium (GIBCO) with 10% FBS (GIBCO) and 5% CO_2 at 37°C .

2.9. MTS assay

The ability of proliferation for tumor cells was detected with MTS reagent (Promega, USA). Generally, cells in 96-well plates were added to the MTS reagent following the manufacturer's instructions. Then, the absorbance was detected with a microplate reader at 490 nm.

2.10. AO/EB staining assay

The 143B and U2OS cells were seeded in a 96-well plate and treated with different treatments incubating for 48 h, then stained by AO/EB dye for 5 min. The results of dying were observed by fluorescence microscope.

2.11. Osteoclast induction and detection assay in vivo and in vitro

Primary bone marrow monocytes (BMM) cells were extracted from mice and cultured in a 96-well plate. Four groups were treated with PBS, ALN ($0.5 \mu\text{M}$), PDA ($50 \mu\text{M}$), and PDA-ALN (PDA $50 \mu\text{M}$; ALN $0.5 \mu\text{M}$), respectively. The mediums were also treated with 30 ng/ml M-CSF and 100 ng/ml RANKL. Then, the cells were stained with TRAP dye (Sigma, USA) and counting the multinucleated cells in each well.

2.12. RT-PCR analysis of osteogenic genes

BMMs were cultured with PDA, ALN, and PDA-ALN. After 7 days of incubation, total RNA was extracted, and cDNA was acquired (TaKaRa, China). Then the cDNA was performed to qPCR analysis (TaKaRa, China). The primer sequences were as follows: TRAF3-FP 5'-TTTCCCGGCCTTACATCATTG-3', TRAF3-RP 5'-GCTTCTTTGAGGTATCCGAGAG-3'; NFATc1-FP 5'-GGAGAGTCCGAGAATCGAGAT-3', NFATc1-RP 5'-TTGCAGCTAGGAAGT-ACGTCT-3'.

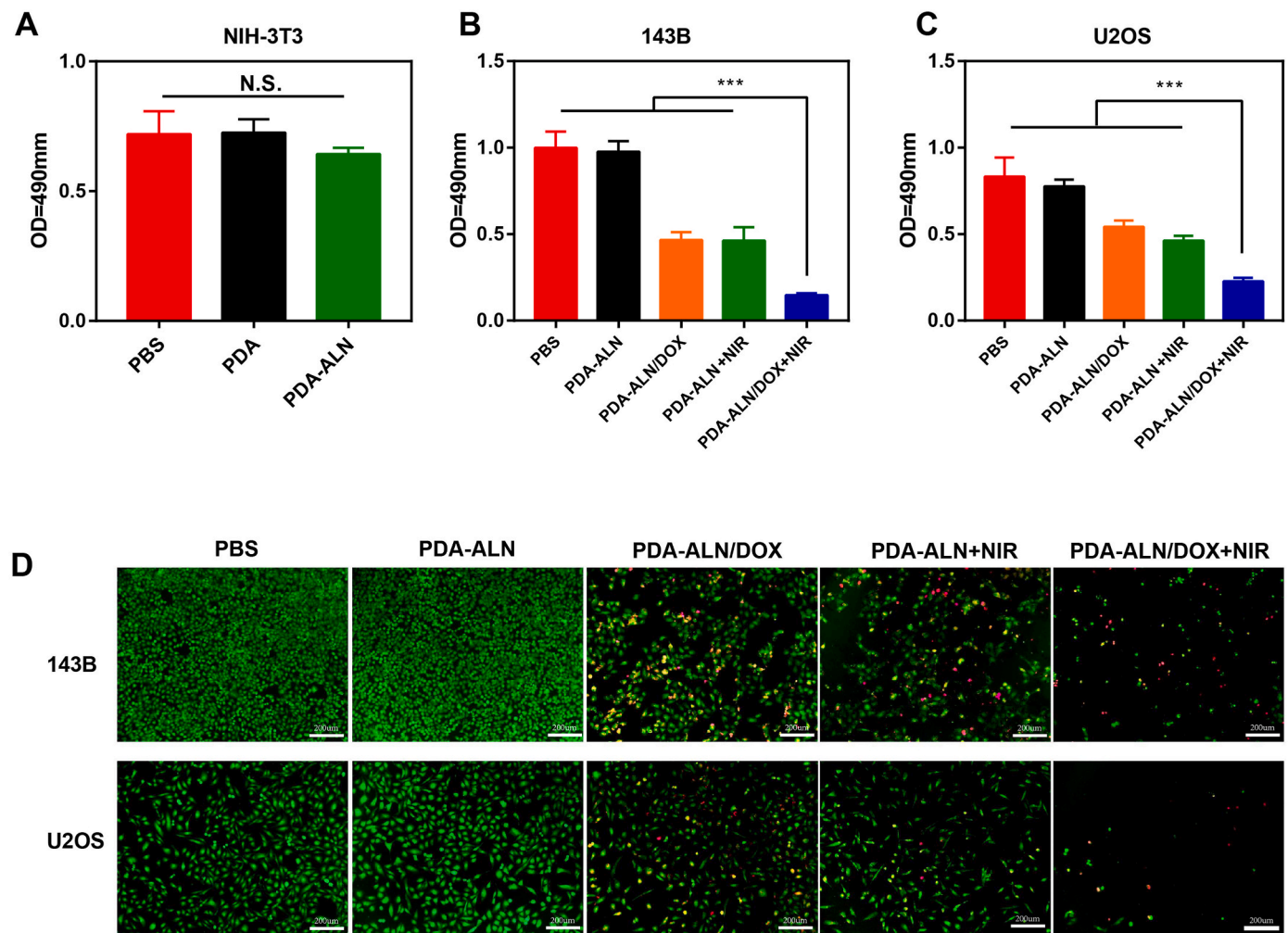


Fig. 2. PDA-ALN/DOX associated photothermal therapy killing of osteosarcoma cells.

(A) The cytotoxicity of PDA on NIH-3T3 cells. (B,C) Chemo-photothermal treatment enhanced the efficiency of killing osteosarcoma cells. (D) AO-EB staining for 143B and U2OS cells after treatments.

* $p < 0.05$, ** $p < 0.01$ and *** $p < 0.001$ analyzed by Student's t-test.

2.13. Western blot analysis of osteogenic proteins

BMMs were cultured with PDA, ALN, and PDA-ALN. After 7 days of incubation, cells were treated with Cytoplasmic Protein Extraction Kit supplemented with protease inhibitor cocktail and protein phosphatase inhibitor (Beyotime Biotechnology). The solution was separated by SDS-PAGE electrophoresis and transferred to PVDF membranes (Millipore, USA), which were incubated with 5% nonfat milk (CST, USA) in PBS for 1 h room temperature at first, then the primary antibody at 4 °C overnight. On the second day, the membranes were incubated with secondary antibodies before washing with PBS-T. The primary antibodies, including anti-NFATc1 and anti-TRAF3, were purchased from Abcam (Cambridge, UK). Finally, the membranes were detected by Odyssey Infrared Imaging System.

2.14. MRI of PDA/Fe and PDA-ALN/Fe in bone tumor mice

All animal experiments were approved by the Ethics Committee of the General Hospital of the Chinese People's Liberation Army and followed the National Institutes of Health guidelines. Four-week-old BALB/c nude mice purchasing from SLAC (Shanghai, China) were injected with 143B-Luc cells in the cavum medullare of tibias. Either PDA/Fe or PDA-ALN/Fe was injected intravenously, respectively. MRI was performed before and 24 h after injection on Bruker 7.0 T magnet.

2.15. Anti-cancer efficacy evaluation of nanoparticles in vivo

The orthotopic tibia tumor-burdened mice were treated with 100 μ l of PBS, PDA-ALN, and PDA-ALN/DOX intravenously, respectively. The groups treated with PDA-ALN (30 mg/kg) and PDA-ALN/DOX (30 mg/kg of PDA concentration; 2.49 mg/kg of DOX concentration) were irradiated by 808 nm NIR laser for 5 min after injection. Repeat the administration and irradiation twice in the following four days. Monitor the tumor growth and record the body weights every day.

2.16. 3D micro-CT of the tumor-bearing tibia in vivo

The tumor-bearing tibias sample were collected and the omnidirectional scanning was started after closing the device door. The rotation speed of the stage was adjusted to 0.6° per second. After the scan, relevant data was evaluated with 3D micro-CT and CTVox programs (Bruker Co.) finally.

2.17. The TUNEL staining assay

The tumors reserved in 4% formalin were embedded in paraffin and sectioned into thick slices, then incubated with proteinase K, TUNEL, and Hoechst 33342 following the manufacturer's instructions (Roche, Mannheim, Germany).

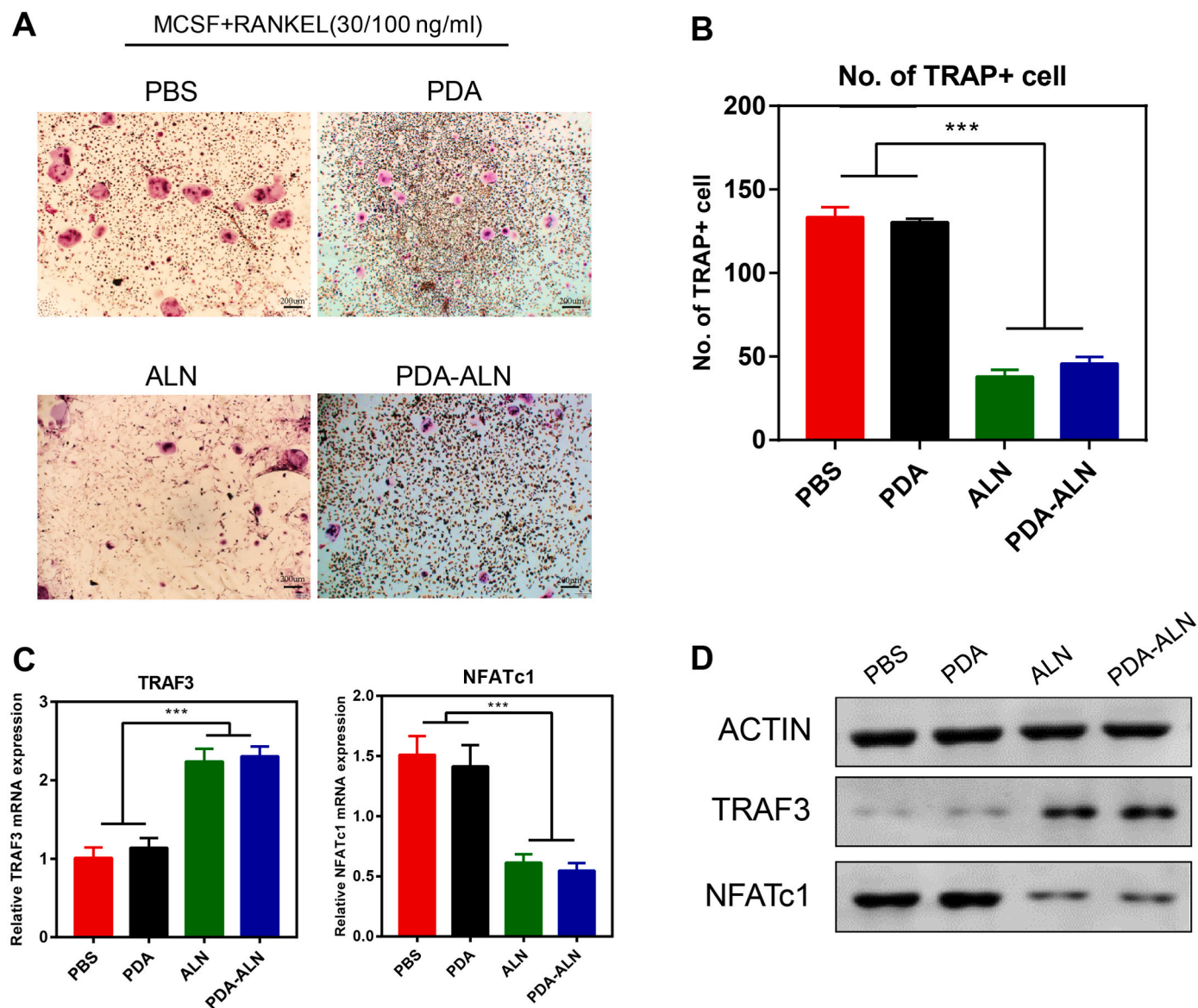


Fig. 3. PDA-ALN inhibits osteoclast differentiation.

(A) TRAP staining images of osteoclastic differentiated BMMs treated with PBS, PDA and PDA-ALN nanoparticles. (B) The number of TRAP-positive multinucleated osteoclast cells with nuclei more than 3 after treatment was counted. (C) TRAF3 and NFATc1 mRNA expressions in BMMs after the same treatment. (D) Western blot analysis of TRAF3 and NFATc1 proteins was performed as the same treatment.

* $p < 0.05$, ** $p < 0.01$ and *** $p < 0.001$ analyzed by Student's t-test.

2.18. H&E staining assay

The major organs preserved in 4% formalin were embedded in paraffin, sectioned into thick slices, and then incubated with hematoxylin and eosin (H&E).

2.19. Statistical analysis

The data presented as the mean \pm SD were analyzed by Prism 7 software. Statistical significance between two samples was determined with two-tailed Student's t-tests.

3. Results and discussion

3.1. Fabrication and characterizations of PDA-ALN and PDA-ALN/DOX

We designed and synthesized a PDA-based bone-targeting

nanoparticle for NIR agents for PTT because of its good biocompatibility, biodegradability, and biosafety [42]. In the synthesis process, PDA was modified with ALN via Michael addition reactions, which could improve the bone-targeted nature of nanoparticles due to the phosphonate group that could bind to the surfaces of HA through chelating with calcium ions [43]. Subsequently, we verified the uniformity of the particle size distribution of PDA by TEM images and DLS analysis (Fig. 1A–F, Fig. S1) for PDA-ALN and PDA-ALN/DOX nanoparticles (with a similar average particle size of 180 nm). We found that all nanoparticles showed a concentrated symmetric distribution of diameters, which did not vary much when modified with small molecule compounds on the PDA surface. To verify the successful loading of the DOX, UV–Vis spectra was performed to detect the characteristic absorption peak at 490 nm. As shown in Fig. 1G, PDA-ALN/DOX had an absorption peak around 490 nm, consistent with DOX, revealing that the nanoparticle PDA-ALN/DOX had been built successfully (8.3% drug loading ratio, w/w). In addition, the photothermal conversion efficiency

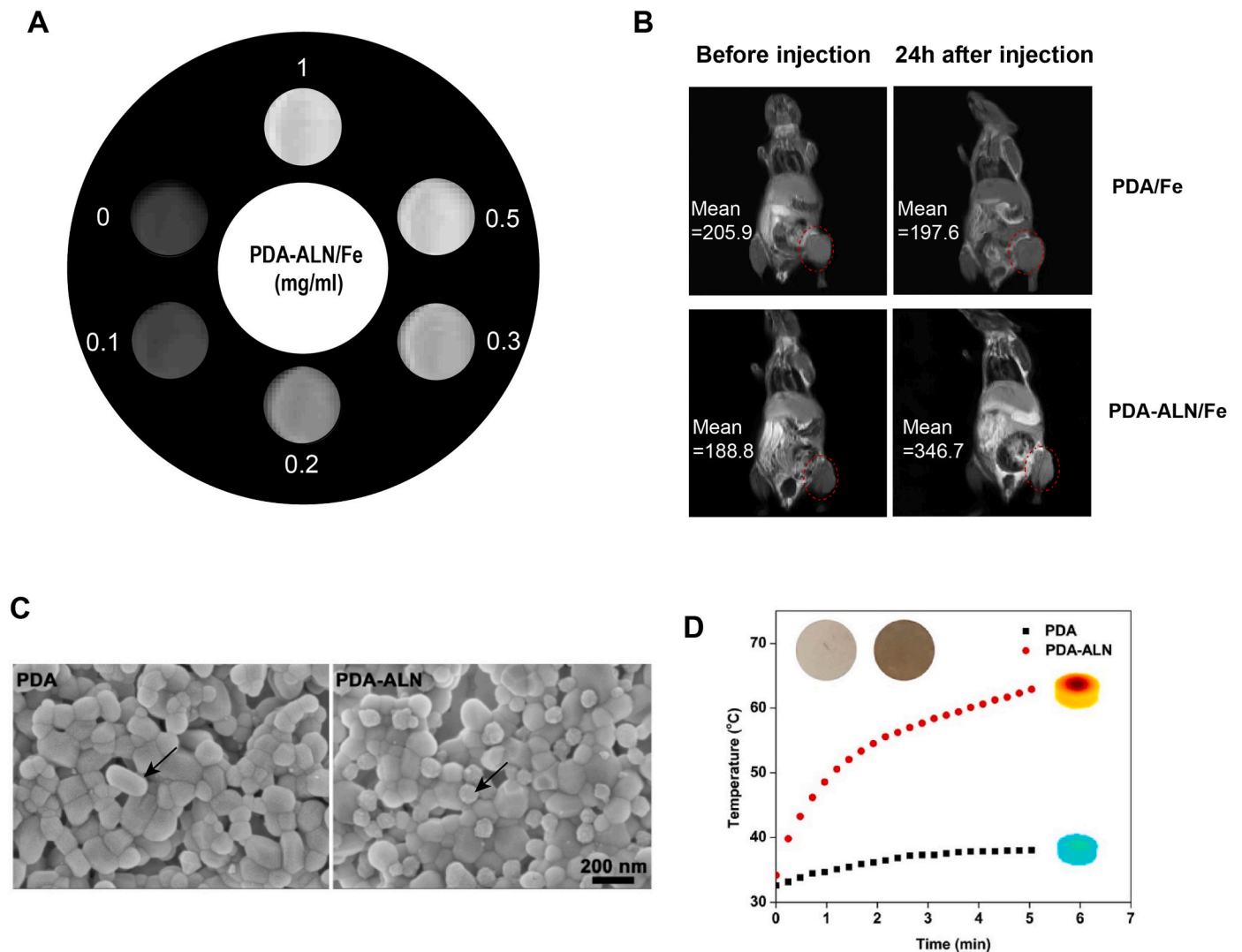


Fig. 4. MRI images and biodistribution of PDA-ALN/Fe.

(A) T1-weighted MR images PDA/Fe at different concentrations in water. (B) T1-weighted MRI images of tibial tumor-bearing mice *in vivo* before and after intravenous injection of PDA/Fe and PDA-ALN/Fe for 24h and tibial tumors were indicated by red arrow. (C) SEM images of HA tablets treated with PDA and PDA-ALN, respectively (black arrow). The nanoparticles were incubated with HA tablets in PBS for 12 h. (D) Temperature changes of PDA- and PDA-ALN-adsorbed HA tablets during NIR irradiation (5.6 W cm⁻², 5 min). Insets are photographs of PDA and PDA-ALN-adsorbed tablets and their thermographs taken at the end of NIR irradiation.

value of PDA-ALN was calculated as 13.7% according to the previous research [44]. Fig. 1H indicated that photothermal heating curves of different concentrations of PDA-ALN irradiated by 808 nm NIR laser at a power density of 3.6 W/cm² and with the concentration increased, the temperature gradually raised. DOX accumulation and release were detected at different times after NIR laser irradiation or without, which indicated NIR irradiation could accelerate the release of DOX in nanoparticles of PDA-ALN/DOX (Fig. 1I). In this section, PDA have plentiful aromatic rings on their surface, making it possible to load chemical drugs, such as DOX, on their surface via π - π stacking and/or hydrogen binding [45]. Under NIR irradiation, hyperthermia on the PDA surface disrupted the interaction between PDA and DOX and speeded up the diffusion of drug molecules. Eventually, the drug was stimulated and released under NIR irradiation.

3.2. Tumor cell internalization and proliferation inhibition *in vitro*

MTS assay was used to monitor the cell proliferation that could substitute for cytotoxicity indirectly. The cell viability rates among PDA, PDA-ALN, and PBS groups had no significant statistical differences,

indicating that PDA-ALN had no apparent toxicity on NIH3T3 cells (Fig. 2A). Furthermore, we evaluated the effects of PDA-ALN/DOX in PTT-killing OS cells *in vitro*. 143B and U2OS cells were given PDA-ALN, the cell viability of which was equal to PBS. When the PDA-ALN group was subjected to NIR laser, the viability of both 143B and U2OS cells was significantly reduced. Then, the DOX-loaded PDA-ALN nanoparticle, PDA-ALN/DOX, was administrated to tumor cells. The tumor cell viability was decreased compared with PBS and PDA-ALN because of the killing effects of DOX. When NIR laser irradiation influenced PDA-ALN/DOX, the tumor cells were killed more efficiently than PDA-ALN/DOX administration only, thanking for the efficiency of thermogenic action of PDA-ALN nanoparticles in PTT. The results of cell viabilities assays indicated that PDA-ALN/DOX with NIR laser irradiation behaved the best on this effect, consistent with AO/EB double staining results (Fig. 2B–D).

3.3. PDA-ALN inhibits osteoclast differentiation

As we all know, vicious cycle played an important role in the bone tumor progression. Moreover, cancer cells can cause osteolytic lesions to

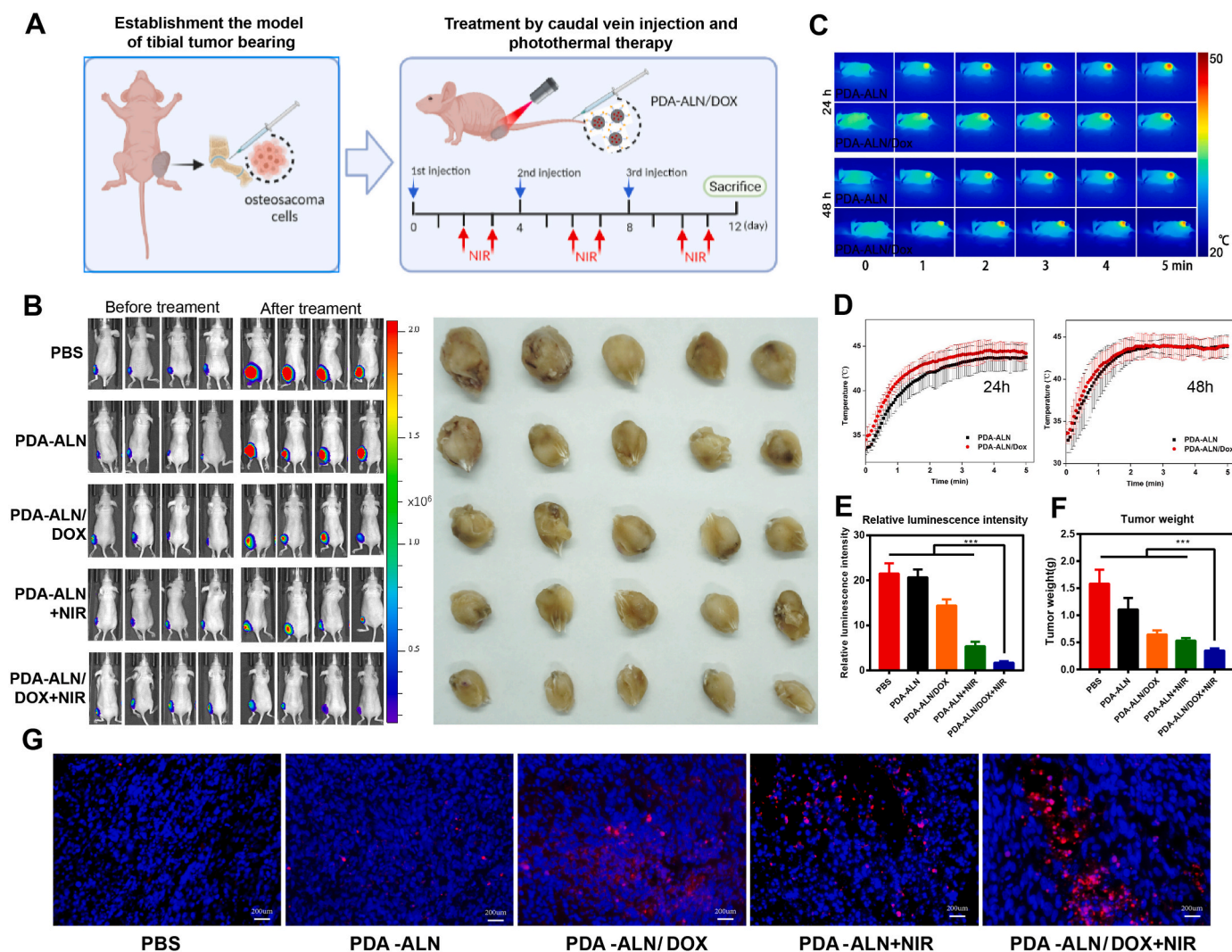


Fig. 5. In vivo treatment of osteosarcoma.

(A) Schematic diagram illustrates the process for PDA-ALN/DOX treatment and NIR irradiation. (B) Luminescence images of tumor bearing mice and photographs of tibial tumors excised from mice. (C) Thermographs of mice taken at the end of NIR irradiation at 24h and 48 h post-injection. (D) The tumor-site temperature changes recorded during the first NIR irradiation (24 h and 48 h after the first injection, 1.0 W cm⁻², 5 min). (E) The average luminescence intensities of tibial tumors before and after treatment. (F) Average weights of tibial tumors excised from mice. (G) Apoptosis (red) of tumor cells after different treatments analyzed by a TUNEL assay. **p* < 0.05 and ****p* < 0.001 analyzed by student's t-test.

promote the net resorption and/or release of growth factors from the bone extracellular matrix [46]. These processes activate a "vicious cycle", leading to disruption of bone integrity and promoting cancer cell growth and migration [46]. Therefore, inhibition of osteoclast differentiation is a significant and effective treatment for bone tumor. To identify the inhibition of osteoclast differentiation effect of PDA-ALN, primary BMMs were cultured with M-CSF (30 ng/ml) and RANKL (100 ng/ml). After 5 days, the cells were stained according to the TRAP kit for identification. The result of osteoclast differentiation of BMMs treated with PDA is similar to PBS. At the same time, ALN and PDA-ALN behaved inversely, this inhibited osteoclast differentiation of BMMs and decreased the TRAP-positive cells significantly compared with PBS and PDA, which suggested that ALN played a vital role in osteoclast differentiation *in vitro* (Fig. 3A and B). Following this, we detected the expression of TRAF3 and NFATc1, the bio-markers of osteoclast differentiation, in transcriptional and translational levels with various agent administration. Similar to the TRAP detection, both TRAF3 and NFATc1 revealed the megascopic difference in ALN and PDA-ALN compared with PBS and PDA. TRAF3 had a noticeable increase in both mRNA and protein expression (Fig. 3C and D) with ALN and PDA-ALN

administration, while NFATc1 performed on the contrary.

3.4. Evaluation of the bone-targeting efficacy *in vivo*

To validate and assess bone targeting and *in vivo* distribution, MRI was performed on iron-loaded PDA nanoparticles (PDA-ALN/Fe). A 7.0 T MRI system received T1 signals before and after the use of NIR agents. An increased T1-weighted MRI signal on the area of the tibial tumor could be observed visibly after PDA-ALN/Fe administration rather than PBS administration, which indicated PDA-ALN/Fe was effective *in vivo* to target bone and distributed around the bone tumors (Fig. 4A and B, Fig. S2).

3.5. Antitumor efficacy and security *in vivo*

To confirm the ability to bone target with HA of synthetic PDA-ALN nanoparticle, the SEM images (Fig. 4C) were taken after incubating with HA tablets. PDA-ALN behaved better on HA tablets binding than PDA administration only, which indicated PDA coupled with ALN could increase the ability of bone target. Then, the nanoparticles were taken to

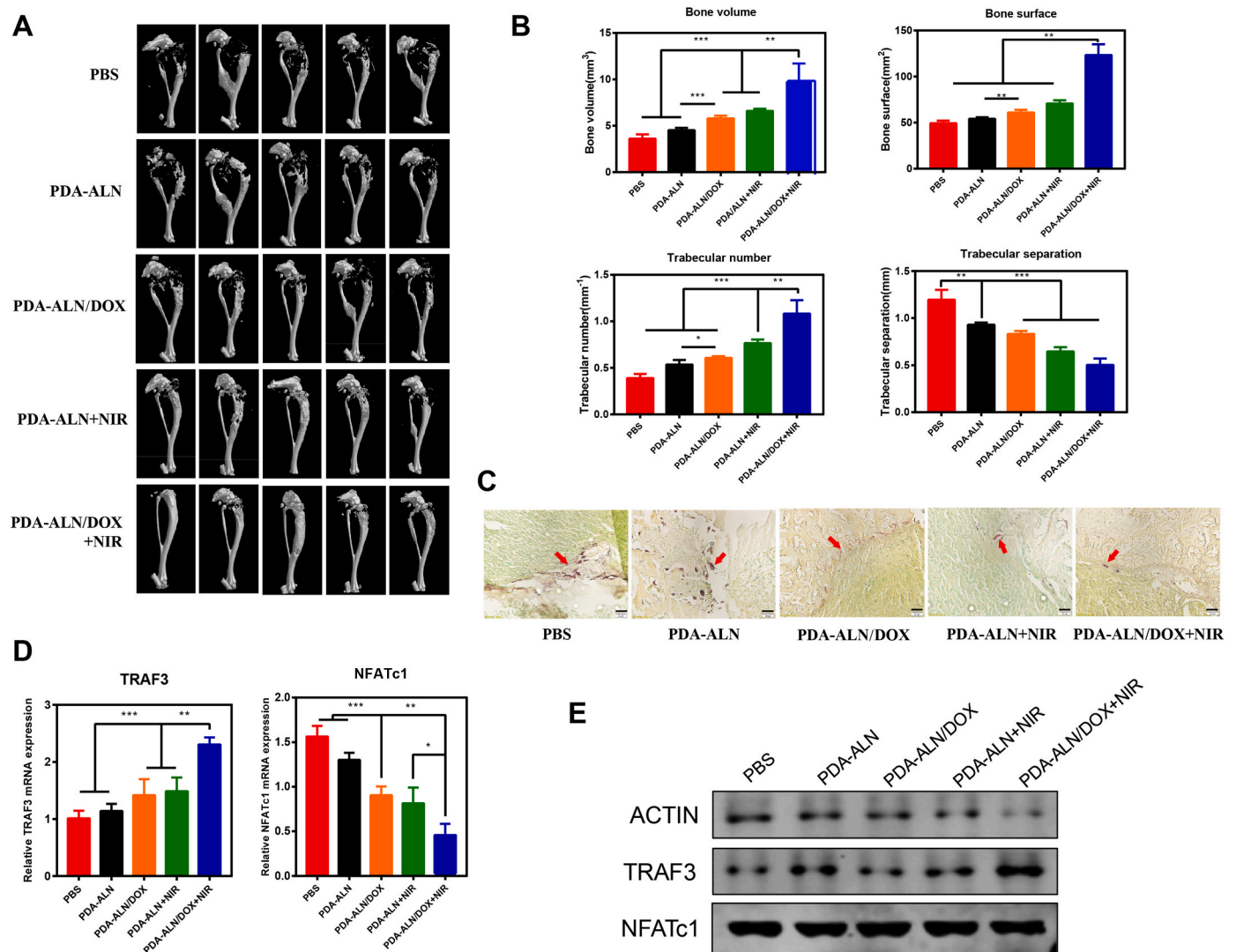


Fig. 6. The inhibition of osteolysis and osteoclast differentiation in osteosarcoma by PDA-ALN/DOX + NIR-mediated treatment.

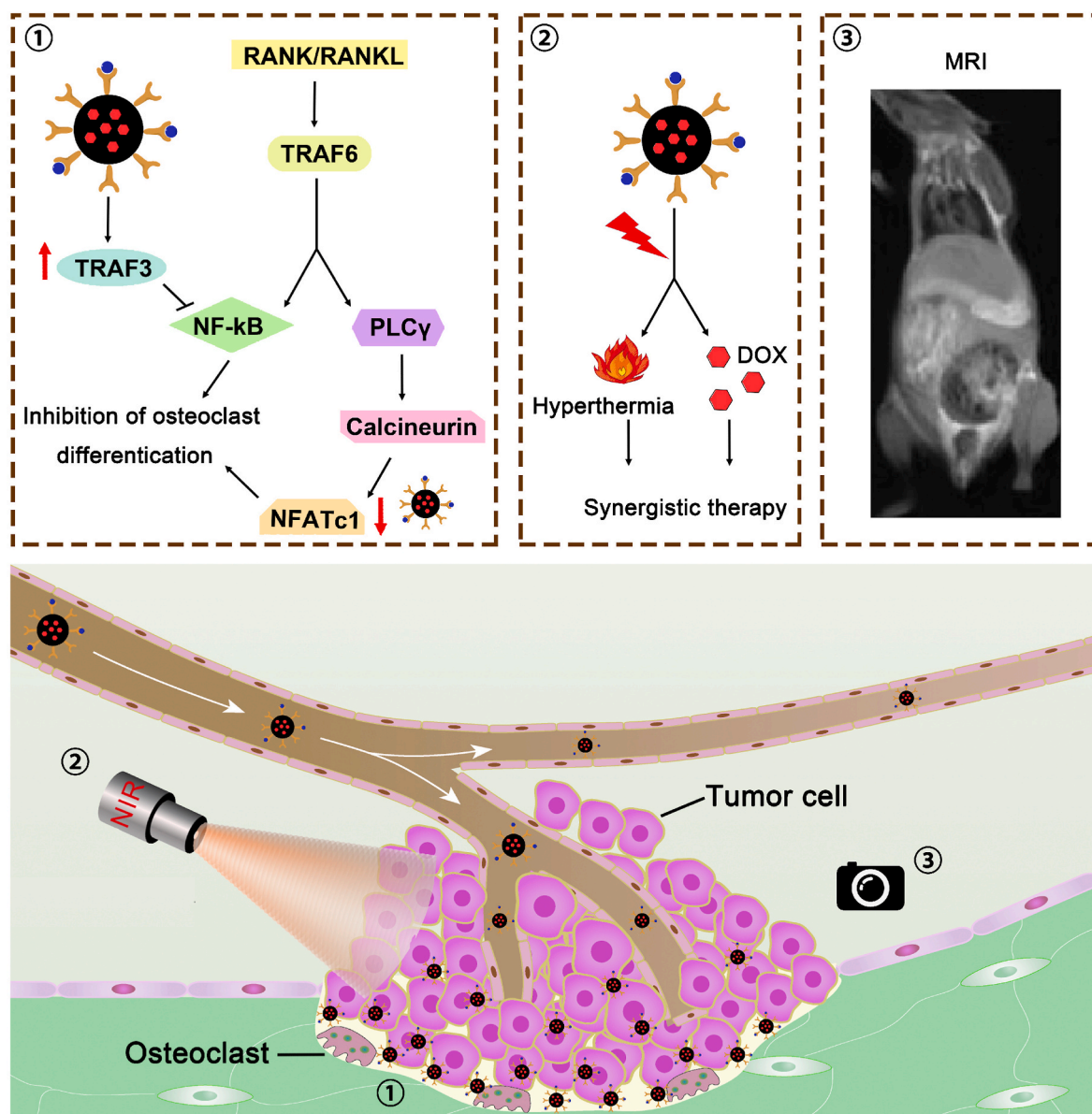
(A) 3D reconstructed image of tibias performed using micro-CT of 143B osteosarcoma-bearing mouse after treatment. (B) Quantitative analysis on the architecture parameters including bone volume, bone surface, trabecular number, and trabecular separation. (C) Representative images of TRAP staining for the five groups of tibial osteoclasts were shown. (D) The mRNA and protein expression level of osteoclast-specific genes including TRAF3 and NFATc1 in the tibial tissues by qRT-PCR. (E) The protein expression level of TRAF3 and NFATc1 in the tibial tissues.

* $p < 0.05$ and *** $p < 0.001$ analyzed by student's t-test.

irradiate with NIR laser at 808 nm to verify the efficiency for PTT and the temperature after irradiation was monitored in real-time that revealed PDA-ALN had the better heating property that could warm rapidly in a short time up to 63 °C with PDA-ALN compared with PDA which could only up-regulate to 38 °C in the same time (Fig. 4D).

After then, orthotopic OS model mice were built to evaluate the effect of PDA-ALN/DOX mediated NIR laser irradiation of PTT *in vivo*. PBS, PDA-ALN, PDA-ALN/DOX were administrated to OS-bearing model mice with the intravenous tail injection (Fig. 5A). Meanwhile, another PDA-ALN and PDA-ALN/DOX were irradiated by NIR light after administration immediately. To value the influence of NIR agents and CPT on the bodyweight of OS-bearing model mice, the mice were weighed and recorded every day after administration and irradiation. As shown in Fig. S3, the bodyweight of mice did not present statistically different and did not change significantly compared with PBS injection, which indicated that nanoparticles and PTT did not damage mice. The fluorescence images of OS-bearing model mice were acquired before and after administration and irradiation. The PDA-ALN/DOX with NIR of PTT had the least fluorescence intensity among the whole OS-bearing

model mice after treatment, while PDA-ALN showed a fairly strong fluorescence similar to PBS injection, which indicated PDA-ALN could not inhibit the growth of OS *in vivo* itself. In the NIR laser of PTT groups (PDA/DOX + NIR and PDA-ALN/DOX + NIR), the average fluorescence intensities were significantly poorer than the PBS injection group, suggesting that CPT could regress the growth of OS provenly (Fig. 5B, E). The tumors from OS-bearing model mice were isolated after 10 days of administration and irradiation, then were arranged as Fig. 5B. The tumor-site temperature of NIR irradiated mice was 43 °C approximately (Fig. 5C and D). Similar to the results of the fluorescence images, the tumors in PDA-ALN/DOX + NIR had the most diminutive average sizes visibly, then the PDA-ALN/DOX and PDA/DOX + NIR. PDA-ALN showed a fair tumor average size similar to PBS injection (Fig. 5E). In addition, the weight of tumors in each treatment group had been detected, which was consistent with tumor fluorescence intensities and sizes (Fig. 5F). After the above detection on tumors, a TUNEL staining assay had been performed to clarify the ability to promote apoptosis. PDA-ALN/DOX + NIR had the most positive apoptosis cells in all treatment groups, indicating that CPT administration and irradiation



Scheme 1. PDA-ALN/DOX-mediated photothermal treatment of osteosarcoma. ALN and DOX released from the nanoparticles inhibit osteoclast differentiation and activation in tumor cells to enhance the efficiency of photothermal killing of osteosarcoma cells. The PDA-ALN/DOX-mediated PTT blocks the vicious cycle between tumor osteosarcoma cell proliferation and bone resorption, resulting in efficient tumor suppression and osteolysis inhibition.

could promote tumor apoptosis to inhibit tumor growth *in vivo* (Fig. 5G).

The osteolysis and bone defect often occurred in OS tumorigenesis and progression. Therefore, OS-bearing model mice were taken to confirm the remitting ability of osteolysis, where 3D micro-CT images of each treatment group, as shown in Fig. 6A, showed smooth remission of osteolysis and defects in bone structure at the OS-bearing location after NIR of PDA-ALN/DOX and CPT compared to any other treatment. Meanwhile, the bone structures were destroyed terribly and obviously. Furthermore, the features of bone structures in OS-bearing model mice were evaluated, including bone volume, bone surface, trabecular numbers (Tb. N.), and the tibia space (Tb. Sp.), in which the tendency of difference in the three indexes aforementioned was consistent (Fig. 6B). Especially, administration of PDA-ALN/DOX and NIR had the maximal bone volume, the most prominent bone surface, and the most trabecular numbers among the whole treatment groups. As for the tibia space, there was a crosscurrent with any other features, in which PDA-ALN/DOX + NIR of CPT had the most comprehensive tibia space.

Above all, the results indicated that the combination therapy of

chemotherapy and PTT with nanoparticles of bone-targeted administration could repress the growth of OS and relieve the osteolysis and bone defect in OS-bearing model mice. Osteoclast differentiation also had been verified and monitored in OS-bearing model mice after administration and irradiation treatments. As shown in Fig. 6C, TRAP staining of tibial osteoclasts become noticeably weaker than others after PDA-ALN/DOX + NIR of CPT. Consistent with the results *in vitro*, the expression of NFATc1 mRNA was decreased significantly treating with both PDA-ALN/DOX administration and NIR laser irradiation and TRAF3 contrasted in the tendency of mRNA expression and protein expression (Fig. 6D and E).

In general, the efficacy of OS treatment had been obviously enhanced in the presence of PDA-ALN/DOX combined with NIR laser irradiation. We further evaluated the hematological toxicity and liver function of mice with different treatments. There were no significant changes in WBC, LYMPH#, RBC, HGB, and HCT. Similar results were also observed for ALT and AST levels in the treated mice (Figs. S4–5). Besides, the histological staining of main organs was performed to detect the toxicity

in vivo after administration of CPT, which suggested no apparent changes in the aforementioned organs implying the NIR agents, including PDA-ALN and PDA-ALN/DOX, had good biocompatibility, biodegradability, and biosecurity (Fig. S6).

4. Conclusion

In summary, we designed and developed a novel nanoparticle, defined as PDA-ALN/DOX, based on the PDA, coupled with ALN and modified with DOX, which behaved well on targeting bone, killing OS both and inhibiting osteoclast differentiation *in vitro* and *in vivo* (Scheme 1). As an agent for NIR laser irradiation of PTT, PDA-ALN/DOX was also modified with DOX, which could become a combined therapy called CPT, which combined PTT with chemotherapy and could improve the current curative effect of OS treatment immensely in clinical. This study could provide a potential CPT agent for OS treatment in clinical.

CRedit authorship contribution statement

Wei-bo Liu: Methodology, Validation, Formal analysis, Data curation, Writing – review & editing. **Su-he Dong:** Conceptualization, Investigation, Writing – review & editing. **Wen-hao Hu:** Validation, Writing – review & editing. **Meng Gao:** Validation, Writing – review & editing. **Teng Li:** Validation, Writing – review & editing. **Quan-bo Ji:** Methodology, Data curation. **Xiao-qing Yang:** Methodology, Data curation. **Deng-bin Qi:** Methodology, Data curation. **Zhen Zhang:** Methodology, Validation. **Ze-Long Song:** Methodology, Validation. **Yu-jie Liu:** Methodology, Validation, Formal analysis, Data curation, Writing – review & editing. **Xue-song Zhang:** Supervision, study design, Funding acquisition.

Declaration of competing interest

We declare that we have no financial and personal relationships with other people or organizations that can inappropriately influence our work, there is no professional or other personal interest of any nature or kind in any product, service and/or company that could be construed as influencing the position presented in, or the review of, the manuscript entitled, “A simple, universal and multifunctional template agent for personalized treatment of bone tumors”.

Appendix A. Supplementary data

Supplementary data to this article can be found online at <https://doi.org/10.1016/j.bioactmat.2021.10.027>.

References

- R.L. Siegel, K.D. Miller, A. Jemal, Cancer statistics, 2019 [J], *CA A Cancer J. Clin.* 69 (1) (2019) 7–34.
- D. Heymann, Metastatic osteosarcoma challenged by regorafenib [J], *Lancet Oncol.* 20 (1) (2019) 12–14.
- J.S. Whelan, L.E. Davis, Osteosarcoma, chondrosarcoma, and chordoma [J], *J. Clin. Oncol.* : official journal of the American Society of Clinical Oncology 36 (2) (2018) 188–193.
- L.M. Kelley, M. Schlegel, S. Hecker-Nolting, et al., Pathological fracture and prognosis of high-grade osteosarcoma of the extremities: an analysis of 2,847 consecutive cooperative osteosarcoma study group (COSS) patients [J], *J. Clin. Oncol.* : official journal of the American Society of Clinical Oncology 38 (8) (2020) 823–833.
- H. Mamdani, S.J. Grethlein, Pulmonary metastases from chondroblastic osteosarcoma [J], *N. Engl. J. Med.* 378 (15) (2018) 1429.
- S. Ekhtiari, K. Chiba, S. Popovic, et al., First case of osteosarcoma in a dinosaur: a multimodal diagnosis [J], *Lancet Oncol.* 21 (8) (2020) 1021–1022.
- E. Kleinerman, Maximum benefit of chemotherapy for osteosarcoma achieved—what are the next steps? [J], *Lancet Oncol.* 17 (10) (2016) 1340–1342.
- F. Fagioli, E. Tirte, Cabozantinib: a new perspective for advanced bone sarcoma [J], *Lancet Oncol.* 21 (3) (2020) 331–332.
- A. Italiano, O. Mir, S. Mathoulin-Pelissier, et al., Cabozantinib in patients with advanced Ewing sarcoma or osteosarcoma (CABONE): a multicentre, single-arm, phase 2 trial [J], *Lancet Oncol.* 21 (3) (2020) 446–455.
- S. Piperno-Neumann, M.C. LE Deley, R. Dini F, et al., Zoledronate in combination with chemotherapy and surgery to treat osteosarcoma (OS2006): a randomised, multicentre, open-label, phase 3 trial [J], *Lancet Oncol.* 17 (8) (2016) 1070–1080.
- T.M. Gibson, S. Mostoufi-Moab, K.L. Stratton, et al., Temporal patterns in the risk of chronic health conditions in survivors of childhood cancer diagnosed 1970–99: a report from the Childhood Cancer Survivor Study cohort [J], *Lancet Oncol.* 19 (12) (2018) 1590–1601.
- S. Pan, J. Yin, L. Yu, et al., 2D MXene-integrated 3D-printing scaffolds for augmented osteosarcoma phototherapy and accelerated tissue reconstruction [J], *Advanced science (Weinheim, Baden-Wuerttemberg, Germany)* 7 (2) (2020) 1901511.
- J. Liao, K. Shi, Y. Jia, et al., Gold nanorods and nanohydroxyapatite hybrid hydrogel for preventing bone tumor recurrence via postoperative photothermal therapy and bone regeneration promotion [J], *Bioactive materials* 6 (8) (2021) 2221–2230.
- Q. Zheng, X. Liu, Y. Zheng, et al., The recent progress on metal-organic frameworks for phototherapy [J], *Chem. Soc. Rev.* 50 (8) (2021) 5086–5125.
- Z. Xie, T. Fan, J. An, et al., Emerging combination strategies with phototherapy in cancer nanomedicine [J], *Chem. Soc. Rev.* 49 (22) (2020) 8065–8087.
- S. Son, J.H. Kim, X. Wang, et al., Multifunctional sonosensitizers in sonodynamic cancer therapy [J], *Chem. Soc. Rev.* 49 (11) (2020) 3244–3261.
- Y. Zhang, L. Zhang, J. Gao, et al., Pro-death or pro-survival: contrasting paradigms on nanomaterial-induced autophagy and exploitations for cancer therapy [J], *Accounts Chem. Res.* 52 (11) (2019) 3164–3176.
- Y. Wang, J. Yang, H. Liu, et al., Osteotropic peptide-mediated bone targeting for photothermal treatment of bone tumors [J], *Biomaterials* 114 (2017) 97–105.
- K. Sahoo, D. Khare, S. Srikrishna, et al., Development of luminescent atacamite nanoclusters for bioimaging and photothermal applications [J], *Nanotechnology* 31 (26) (2020) 265102.
- G. Feng, G.Q. Zhang, D. Ding, Design of superior phototheranostic agents guided by Jablonski diagrams [J], *Chem. Soc. Rev.* 49 (22) (2020) 8179–8234.
- L. Zhou, F. Lv, L. Liu, et al., Water-soluble conjugated organic molecules as optical and electrochemical materials for interdisciplinary biological applications [J], *Accounts Chem. Res.* 52 (11) (2019) 3211–3222.
- B. Yang, J. Yin, Y. Chen, et al., 2D-Black-Phosphorus-Reinforced 3D-printed scaffolds: A stepwise countermeasure for osteosarcoma [J], *Adv. Mater.* 30 (10) (2018), e201705611.
- N. Panwar, A.M. Soehartono, K.K. Chan, et al., Nanocarbons for biology and medicine: sensing, imaging, and drug delivery [J], *Chem. Rev.* 119 (16) (2019) 9559–9656.
- N. Fabri-Faja, O. Calvo-Lozano, P. Dey, et al., Early sepsis diagnosis via protein and miRNA biomarkers using a novel point-of-care photonic biosensor [J], *Anal. Chim. Acta* 1077 (2019) 232–242.
- Q. Yang, H. Yin, T. Xu, et al., Engineering 2D mesoporous Silica@MXene-integrated 3D-printing scaffolds for combinatory osteosarcoma therapy and NO-augmented bone regeneration [J], *Small* 16 (14) (2020), e1906814.
- S. He, J. Song, J. Qu, et al., Crucial breakthrough of second near-infrared biological window fluorophores: design and synthesis toward multimodal imaging and theranostics [J], *Chem. Soc. Rev.* 47 (12) (2018) 4258–4278.
- M. Quadros, M. Momin, G. Verma, Design strategies and evolving role of biomaterial assisted treatment of osteosarcoma [J], *Materials science & engineering C, Materials for biological applications* 121 (2021) 111875.
- Y. Yang, X. Fan, L. Li, et al., Semiconducting polymer nanoparticles as theranostic system for near-infrared-II fluorescence imaging and photothermal therapy under safe laser fluence [J], *ACS Nano* 14 (2) (2020) 2509–2521.
- L. Zhang, J. Zhang, L. Xu, et al., NIR responsive tumor vaccine in situ for photothermal ablation and chemotherapy to trigger robust antitumor immune responses [J], *J. Nanobiotechnol.* 19 (1) (2021) 142.
- D. Yang, B. Zhou, G. Han, et al., Flexible transparent polypyrrole-decorated MXene-based film with excellent photothermal energy conversion performance [J], *ACS Appl. Mater. Interfaces* 13 (7) (2021) 8909–8918.
- Z. Xu, H. Huang, X. Xiong, et al., A near-infrared light-responsive extracellular vesicle as a “Trojan horse” for tumor deep penetration and imaging-guided therapy [J], *Biomaterials* 269 (2021) 120647.
- K. Chen, Q. Li, X. Zhao, et al., Biocompatible melanin based theranostic agent for *in vivo* detection and ablation of orthotopic micro-hepatocellular carcinoma [J], *Biomaterials science* 8 (15) (2020) 4322–4333.
- J. Li, Z. Zhang, H. Deng, et al., Cinobufagin-loaded and folic acid-modified polydopamine nanomedicine combined with photothermal therapy for the treatment of lung cancer [J], *Frontiers in chemistry* 9 (2021) 637754.
- Y. Li, Y. Jin, W. Guo, et al., Decomposable black phosphorus nano-assembly for controlled delivery of cisplatin and inhibition of breast cancer metastasis [J], *J. Contr. Release : official journal of the Controlled Release Society* 335 (2021) 59–74.
- Y. Xi, X. Xie, Y. Peng, et al., DNAzyme-adsorbed polydopamine@MnO(2) core-shell nanocomposites for enhanced photothermal therapy via the self-activated suppression of heat shock protein 70 [J], *Nanoscale* 13 (9) (2021) 5125–5135.
- S. Xue, X. Zhou, W. Sang, et al., Cartilage-targeting peptide-modified dual-drug delivery nanoplatfrom with NIR laser response for osteoarthritis therapy [J], *Bioactive materials* 6 (8) (2021) 2372–2389.
- Y. Zeng, M. Zhou, L. Chen, et al., Alendronate loaded graphene oxide functionalized collagen sponge for the dual effects of osteogenesis and anti-osteoclastogenesis in osteoporotic rats [J], *Bioactive materials* 5 (4) (2020) 859–870.

- [38] A. Plan Sangnier, R. Aupaure, L. Motte, et al., Hybrid Au@alendronate nanoparticles as dual chemo-photothermal agent for combined cancer treatment [J], *Beilstein J. Nanotechnol.* 9 (2018) 2947–2952.
- [39] Y. Wang, Q. Huang, X. He, et al., Multifunctional melanin-like nanoparticles for bone-targeted chemo-photothermal therapy of malignant bone tumors and osteolysis [J], *Biomaterials* 183 (2018) 10–19.
- [40] X. Li, H. Li, C. Zhang, et al., Intelligent nanogels with self-adaptive responsiveness for improved tumor drug delivery and augmented chemotherapy [J], *Bioactive materials* 6 (10) (2021) 3473–3484.
- [41] H. Wang, S. Xu, D. Fan, et al., Multifunctional microcapsules: a theranostic agent for US/MR/PAT multi-modality imaging and synergistic chemo-photothermal osteosarcoma therapy, [J]. *Bioactive materials* 7 (2022) 453–465.
- [42] J. Lu, L. Cai, Y. Dai, et al., Polydopamine-based nanoparticles for photothermal therapy/chemotherapy and their synergistic therapy with autophagy inhibitor to promote antitumor treatment [J], *Chem. Rec.* 21 (4) (2021) 781–796.
- [43] Y. Yan, X. Gao, S. Zhang, et al., A carboxyl-terminated dendrimer enables osteolytic lesion targeting and photothermal ablation of malignant bone tumors [J], *ACS Appl. Mater. Interfaces* 11 (1) (2019) 160–168.
- [44] Y. Zou, X. Chen, P. Yang, et al., Regulating the absorption spectrum of polydopamine [J], *Science advances* 6 (36) (2020).
- [45] Y. Chen, F. Zhang, Q. Wang, et al., The synthesis of LA-Fe(3)O(4)@PDA-PEG-DOX for photothermal therapy-chemotherapy [J], *Dalton Trans.* 47 (7) (2018) 2435–2443. Cambridge, England : 2003.
- [46] L. Xing, E.M. Schwarz, B.F. Boyce, Osteoclast precursors, RANKL/RANK, and immunology [J], *Immunol. Rev.* 208 (2005) 19–29.